JCTC Journal of Chemical Theory and Computation

Ab Initio Finite-Temperature Electronic Absorption Spectrum of Formamide

Nicholas A. Besley[†] and Nikos L. Doltsinis*[,‡]

School of Chemistry, University of Nottingham, Nottingham, NG7 2RD, United Kingdom, and Lehrstuhl für Theoretische Chemie, Ruhr-Universität Bochum, Bochum, D-44780 Germany

Abstract: A combination of Car−Parrinello molecular dynamics (CP−MD) and high-level ab initio quantum chemical calculations has been used to calculate the electronic absorption spectrum of formamide at finite temperatures. Thermally broadened spectra have been obtained by averaging over a large number of single-point multireference configuration interaction excitation energies calculated for geometries sampled from a CP−MD simulation. Electronic excitation spectra of possible contaminants ammonia and formamidic acid have also been computed. Ammonia exhibits a strong peak in the shoulder region of the experimental formamide spectrum at 6.5 eV, and formamidic acid has a strong absorption above 7.5 eV. The calculations reproduce the shape of the experimental absorption spectrum, in particular, the low-energy shoulder of the main peak, and demonstrate how finite-temperature electronic absorption spectra can be computed from first principles.

1. Introduction

A major goal of current research in molecular biology is the determination and understanding of protein structure. X-ray crystallography can determine protein structure at the atomic level. However, many proteins cannot be crystallized, and there may be differences between the crystal and solvated structures. These disadvantages coupled with time-resolved spectroscopy, which can monitor the evolution of protein structure, have led to continued interest in spectroscopic probes of protein structure.[1,2]

Electronic circular dichroism (CD) spectroscopy is used extensively as a measure of the helical content of proteins. Theoretical calculations of protein CD hold the key to establishing and quantifying the link between the measured spectra and the underlying structural information. To date, the most accurate theoretical calculations of protein circular dichroism spectroscopy use small amides as models of the backbone chromophore.[3] This role as a model for the repeating unit in the protein backbone has motivated many studies into the electronic structure of amides. In particular, many theoretical and experimental investigations of the excited states of formamide in the gas phase[4−15] and in solution[4,15−22] have been reported. In addition to characterizing the spectroscopy of an important system, these studies provide a basis for improving our understanding and simulation of the spectroscopy of proteins.

In the gas phase,[13] the electronic spectrum of formamide is dominated by an intense band at 7.4 eV, often labeled the V_1 band, arising from a $\pi_{nb}\pi^*$ (nonbonding π orbital to antibonding π^* orbital) transition. At about 5.5 eV is a much weaker band arising from the $n\pi^*$ (lone pair on an oxygen to an antibonding π^* orbital) transition. The spectrum is also characterized by a number of sharp peaks that are attributed to Rydberg excitations. At a higher energy is the Q band that was originally assigned to a $\pi_b\pi^*$ excitation, although later work has shown it to arise from a superposition of Rydberg excitations.[14]

In recent years, there has been a number of theoretical studies of the excited states of formamide employing a range of methodologies. Multireference configuration interaction (MRCI) calculations were reported by Hirst et al.[10] These provided an accurate description of the Rydberg states, but

* Corresponding author e-mail: nikos.doltsinis@theochem.rub.de.
† University of Nottingham.
‡ Ruhr-Universität Bochum.

Electronic Absorption Spectrum of Formamide

J. Chem. Theory Comput., Vol. 2, No. 6, 2006 **1599**

the predicted $\pi_{nb}\pi^*$ excitation energy was too high. This was attributed to Rydberg-valence mixing and was not improved significantly with the use of a larger active space. Rydberg-valence mixing occurs because the average state MRCI calculation includes a number of Rydberg states in addition to the valence $n\pi^*$ and $\pi_{nb}\pi^*$ states. The Rydberg states are optimized at the "cost" of the valence states, resulting in the valence states being too diffuse with corresponding energies that are too high. The complete active space self-consistent field with multiconfigurational perturbation theory (CASSCF/CASPT2) study of Serrano-Andrés and Fülscher overcame this problem with a two-step procedure comprising a calculation of the Rydberg state energies followed by a subsequent calculation with the Rydberg states "deleted" to determine the valence state properties.[11] These calculations predicted a value of 7.41 eV for the $\pi_{nb}\pi^*$ excitation energy, in agreement with experimental results.

These calculations represent each electronic transition with a single energy and oscillator strength. The direct calculation of electronic spectra represents an important challenge for theory. Broadening of the spectral lines can occur through thermal and electronic effects, resulting in the spectral bands observed in experimental results. The electronic spectrum of formamide has been simulated using a combination of molecular dynamics and quantum chemical calculations to model the thermal broadening of the spectral lines. Doltsinis and Sprik[14] used a combination of Car–Parrinello molecular dynamics (CP–MD) and time-dependent density functional theory (TDDFT) to calculate the electronic spectrum of formamide at room temperature. However, the sampling of configuration space in this study was poor, and the TDDFT Rydberg excitation energies were lacking the important Rydberg corrections. Later work[15] used classical molecular dynamics simulation with TDDFT to model the electronic spectra of a number of amides, including formamide. Both of these studies reproduced important spectral features observed in experimental results but failed to explain certain characteristics of the experimental spectra such as the low-energy shoulder of the main peak around 7.4 eV.

In this work, we reinvestigate the excited states of formamide with MRCI. An improved description of thermal broadening is achieved by averaging over a large number of finite temperature configurations sampled from CP–MD simulations. The thermally averaged results using CP–MD will be compared in detail to those obtained using a classical force field. To partially mimic nuclear quantum effects which smear out the distribution function of the atomic nuclei, we have also carried out CP–MD simulations at increased temperatures[23,24] and studied the effect on the absorption spectrum. Furthermore, we discuss for the first time the absorption spectra of the possible contaminants ammonia and formamidic acid.

2. Computational Details

CP–MD[25,26] simulations of formamide have been carried out at three different temperatures, 300, 400, and 500 K. The calculations were performed in a periodically repeated orthorhombic unit cell of size $10 \times 8 \times 10$ Å using the BLYP exchange-correlation functional[27,28] and a plane-wave

basis truncated at 70 Ry in conjunction with Troullier–Martins pseudopotentials.[29] The system was first brought to thermal equilibrium in a thermostated run over more than 2 ps using a Nosé–Hoover chain[30,31] for each degree of freedom. In the production run of about 15 ps in length, a single Nosé–Hoover chain was used for the whole system to reproduce the canonical ensemble. The propagation of both the fictitious electronic and the nuclear degrees of freedom was carried out with a time step of 4 au; a fictitious mass of 400 au was ascribed to the former. Analogous CP–MD simulations were performed for gas-phase ammonia using the same settings as those for formamide. Merely the unit cell was changed to a simple cubic box of length 9 Å. From each production run, a set of 100 molecular structures was extracted at intervals of 1000 MD steps (roughly 100 fs).

Classical molecular dynamics simulations were performed using the CHARMM program[32] with the CHARMM22 all-hydrogen parameters.[33] All simulations had a time step of 1 fs and consisted of a heating time of 6 ps in which the temperature was raised from 0 to 300 K followed by an equilibrium period of 12 ps. In the first simulation, denoted class-short, 100 structures were drawn at 20 fs intervals from a 200 ps simulation. The second set of 100 structures, denoted class-long, were taken from 10 independent 200 ps simulations at 2 ps intervals. These classical simulations are described in more detail elsewhere.[15]

We would like to emphasize at this point that we obtain thermally broadened electronic excitation spectra by averaging over 100 vertical excitation spectra calculated at the different geometries sampled from a ground-state trajectory. A full quantum-mechanical treatment would also require calculation of the overlap between the nuclear wave functions of the ground state and all excited states. However, this is currently unfeasible for the large number of electronic states and structures considered here.

Excited-state calculations were performed using the MOL-PRO suite of programs.[34] Reference orbitals for the MRCI calculations were obtained from state averaged multi-configurational self-consistent field calculations (MCSCF). The MP2/6-31+G** equilibrium geometry with C_s symmetry from an earlier study[10] was used. The (9,0;16,6) active space comprising nine a′ and zero a″ closed orbitals with seven a′ and six a″ active orbitals was chosen. The active a′ orbitals include the n, 3s, $3p_x$, $3p_y$, $3d_{xy}$, $3d_{x^2-y^2}$, and $3d_{z^2}$ orbitals, while the active a″ orbitals are the π_b, π_{nb}, π^*, $3p_z$, $3d_{xz}$, and $3d_{yz}$ orbitals (with formamide in the xy plane). In the MRCI calculations, 10 A′ states and nine A″ states were calculated using the projection procedure introduced by Knowles and Werner.[35] However, these calculations give poor excitation energies and properties for the $n\pi^*$ and π_{nb}-3s states. The source of this problem lies with the MCSCF reference calculation, which predicts the $n\pi^*$ state to lie above the π_{nb}3s state. To obtain accurate values for these states, a second state averaged MRCI calculation over the two lowest A″ states was performed. The d-aug-cc-pVDZ and d-aug-cc-pVTZ basis sets[36−38] were used for these calculations. Structures drawn from molecular dynamics simulations have C_1 symmetry. For these calculations, the projection procedure was employed to determine the lowest

Table 1. MRCI/d-aug-cc-pVDZ Excitation Energies, ΔE (in eV); Permanent and Transition Dipole Moments, μ and μ^T (in debye); and Oscillator Strengths, σ, for Formamide[a]

state	ΔE	μ_x	μ_y	μ_z	$\lvert\mu\rvert$	μ_x^T	μ_y^T	μ_z^T	σ	assignment
1A′		4.31	−1.13	0.00	4.46					G. S.
2A′	6.41	−3.13	−0.20	0.00	3.13	−0.03	0.02	0.00	0.000	n3s
3A′	7.09	1.43	3.17	0.00	3.48	1.17	−1.10	0.00	0.069	n3p
4A′	7.33	3.14	−3.07	0.00	4.39	−2.17	−1.02	0.00	0.160	$\pi_{nb}\pi^*$
5A′	7.44	−0.16	−0.18	0.00	0.24	−1.33	0.61	0.00	0.060	n3p
6A′	7.76	−0.10	3.49	0.00	3.49	−1.61	−0.30	0.00	0.079	π_{nb}3p
7A′	8.21	−0.53	−1.45	0.00	1.54	0.02	−0.18	0.00	0.001	n3d
8A′	8.33	−0.70	2.40	0.00	2.50	0.37	0.08	0.00	0.004	π_{nb}3d
9A′	8.40	−7.92	−0.33	0.00	7.93	0.96	0.16	0.00	0.030	n3d
10A′	8.53	6.35	0.81	0.00	6.40	−0.46	0.00	0.00	0.007	n3d
1A″	5.76	1.83	−0.24	0.00	1.84	0.00	0.00	0.09	0.000	n π^*
2A″	6.11	−3.96	−0.15	0.00	3.96	0.00	0.00	−0.98	0.022	π_{nb}3s
3A″	7.11	−3.52	0.37	0.00	3.54	0.00	0.00	−0.15	0.006	π_{nb}3p
4A″	7.46	4.75	−0.04	0.00	4.75	0.00	0.00	−0.41	0.005	π_{nb}3p
5A″	7.50	0.17	1.53	0.00	1.54	0.00	0.00	−0.47	0.006	n3p
6A″	8.15	−4.93	0.12	0.00	4.93	0.00	0.00	0.20	0.001	π_{nb}3d
7A″	8.18	0.32	0.28	0.00	0.42	0.00	0.00	−0.28	0.002	π_{nb}3d
8A″	8.42	3.55	−0.32	0.00	3.56	0.00	0.00	−0.17	0.001	n3d
9A″	8.47	2.24	4.56	0.00	5.08	0.00	0.00	−0.29	0.003	π_{nb}3d

[a] The coordinates (in bohr) of the C, N, and O atoms are (−0.16, −0.78, 0), (2.17, 0.32, 0), and (−2.16, 0.39, 0), respectively.

20 states. Again, the poor MCSCF reference led to problems for the $n\pi^*$ and π_{nb}3s states. The excitation energies and transition dipole moments for the $n\pi^*$, π_{nb}3s, and n3s states were taken from separate state averaged MRCI calculations over the four lowest states. All calculations used the d-aug-cc-pVDZ basis set.

In addition to formamide, calculations have also been performed to assess the effect of likely contaminants on the absorption spectrum. The excited states of formamidic acid have been computed at the ground-state equilibrium MP2/6-31+G** structure with C_s symmetry. A similar protocol to formamide was used, with the (9,0;16,6) active space and d-aug-cc-pVDZ basis set. For formamidic acid, averaging over structural snapshots drawn from MD simulations was not performed and a spectrum was generated by representing transitions with a Gaussian function with a bandwidth of 0.2 eV to mimic the thermal broadening. Ammonia was also studied at the MRCI/d-aug-cc-pVDZ level. An active space of (2;10) was chosen and the lowest five states computed using the projection procedure. The electronic absorption spectrum was generated on the basis of 100 snapshots drawn from the CP−MD simulation.

3. Results and Discussion

Table 1 shows the computed excitation energies and permanent and transition dipole moments for the equilibrium (C_s) structure computed with the d-aug-cc-pVDZ basis set. The main focus of studies of amide excited states is the $\pi_{nb}\pi^*$ state because this transition dominates the electronic absorption and CD spectra. The calculations predict an excitation energy of 7.33 eV. This lies close to the value from the experiment of 7.4 eV. Previous studies have shown accurate calculation of this excited state to be problematic because of Rydberg-valence mixing.[10,11] Our calculations differ from this previous work because a much larger basis set is used.

In particular, the d-aug-cc-pVDZ contains a number of diffuse basis functions that are appropriate for describing Rydberg states. This indicates that the Rydberg-valence mixing and associated poor description of the $\pi_{nb}\pi^*$ excited state is an artifact of the small basis set. This is reasonable because a large basis set should be sufficiently flexible to describe both Rydberg and valence states and, in conjunction with MRCI with a large active space, should be accurate. The calculations predict $\pi_{nb}\pi^*$ to be the most intense, although the computed oscillator strength is less than the estimated experimental value in solution.[11]

The other important valence state is the $n\pi^*$ state. This state is weak and difficult to characterize in experiments. The predicted excitation energy of 5.76 eV is in agreement with experimental and previous calculations.[11,19] Most of the intensities for the remaining Rydberg states are low. The exceptions are the π_{nb}3s and n3p states on the low-energy side of the $\pi_{nb}\pi^*$ state and n3p, π_{nb}3p, and n3d excitations on the high-energy side. Table 2 shows results for the larger d-aug-cc-pVTZ basis set. There is little change in the calculated excitation energies. However, for some of the higher-lying Rydberg states, there are some significant changes in the computed dipole moments. This indicates that there are not sufficient basis functions in the smaller basis set to describe these states. Overall, there is good agreement between the absorption spectra predicted with the two basis sets, and the smaller d-aug-cc-pVDZ basis set is used in subsequent calculations.

Figure 1 shows the computed spectra based on CP−MD simulations at 300, 400, and 500 K with the experimental spectrum reported by Gingell et al.[13] shown in bold. At 300 K, the spectrum generally has the correct shape with an intense band at the correct energy arising predominantly from the $\pi_{nb}\pi^*$ transition. The calculated spectrum also shows the formation of a shoulder between 6 and 7 eV comprising π3s

Table 2. MRCI/d-aug-cc-pVTZ Excitation Energies, ΔE (in eV); Permanent and Transition Dipole Moments, μ and μ^{T} (in debye); and Oscillator Strengths, σ, for Formamide[a]

state	ΔE	μ_x	μ_y	μ_z	$|\mu|$	μ_x^{T}	μ_y^{T}	μ_z^{T}	σ	assignment
1A′		4.31	−1.15	0.00	4.46					G. S.
2A′	6.45	−3.10	−0.14	0.00	3.10	−0.01	0.02	0.00	0.000	n3s
3A′	7.13	1.21	3.13	0.00	3.35	1.10	−1.11	0.00	0.066	n3p
4A′	7.40	3.37	−2.88	0.00	4.43	−2.13	−0.97	0.00	0.154	$\pi_{\mathrm{nb}}\pi^*$
5A′	7.49	−0.56	−0.58	0.00	0.81	1.48	−0.54	0.00	0.071	n3p
6A′	7.86	0.16	3.96	0.00	3.96	−1.41	−0.35	0.00	0.063	π_{nb}3p
7A′	8.25	−0.65	−1.15	0.00	1.32	0.01	−0.17	0.00	0.001	n3d
8A′	8.34	1.77	1.93	0.00	2.61	0.02	0.04	0.00	0.000	π_{nb}3d
9A′	8.49	−2.47	−0.24	0.00	2.48	0.81	0.25	0.00	0.023	n3d
10A′	8.58	1.56	0.72	0.00	1.72	0.97	0.10	0.00	0.031	n3d
1A″	5.76	1.82	−0.20	0.00	1.84	0.00	0.00	0.08	0.000	$n\,\pi^*$
2A″	6.17	−3.97	−0.92	0.00	3.97	0.00	0.00	−0.98	0.023	π_{nb}3s
3A″	7.07	−0.32	−0.66	0.00	0.73	0.00	0.00	−0.14	0.001	π_{nb}3p
4A″	7.52	4.62	0.07	0.00	4.63	0.00	0.00	−0.37	0.004	π_{nb}3p
5A″	7.54	0.15	1.53	0.00	1.54	0.00	0.00	0.50	0.007	n3p
6A″	8.22	2.36	0.19	0.00	2.36	0.00	0.00	−0.46	0.006	π_{nb}3d
7A″	8.26	0.58	1.27	0.00	1.39	0.00	0.00	−0.12	0.000	π_{nb}3d
8A″	8.45	2.88	−0.52	0.00	2.92	0.00	0.00	−0.12	0.000	n3d
9A″	8.54	1.08	3.89	0.00	4.03	0.00	0.00	−0.15	0.001	π_{nb}3d

[a] The coordinates (in bohr) of the C, N, and O atoms are (−0.16, −0.78, 0), (2.17, 0.32, 0), and (−2.16, 0.39, 0), respectively.
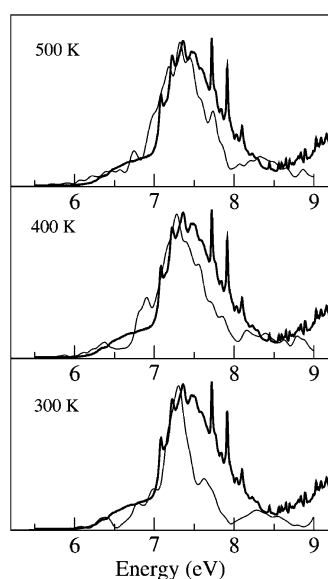
Figure 1. Theoretical simulations of the electronic absorption spectrum of formamide based on CP-MD simulations at different temperatures. The experimental spectrum[13] is shown in bold.

and n3p transitions. Although, the bands arising from these excitations are distinct and have not merged. On the high-energy side of the $\pi_{\mathrm{nb}}\pi^*$ band, there is little evidence of the sharp Rydberg bands observed in experimental results. The calculations only include the lowest 20 states, so there is no attempt to describe the spectrum above 8.5 eV. However, the main deficiency in the computed spectrum is that the $\pi_{\mathrm{nb}}\pi^*$ band is too narrow. At the higher temperatures, there is significant further broadening on the $\pi_{\mathrm{nb}}\pi^*$ band. At 500 K, there is reasonable agreement between the calculated and experimental spectra. Furthermore, the π3s and n3p bands merge, producing a broad shoulder on the low-energy side of the $\pi_{\mathrm{nb}}\pi^*$ band. On the high-energy side of the $\pi_{\mathrm{nb}}\pi^*$

band, the sharp bands corresponding to Rydberg excitations can be distinguished. We should bear in mind, at this point, that in the CP−MD simulations the atomic nuclei are treated as classical particles. Compared to a full quantum-mechanical description, the thermal distribution of classical nuclei is too narrow. However, it has been demonstrated previously[23,24] that nuclear quantum fluctuations can be emulated very well by CP−MD simulations at a higher temperature. It is not clear a priori, though, how to map the temperature of a classical simulation onto the real (quantum) temperature. Our observation that the classical simulation at 500 K yields closer agreement with experimental results than the lower temperature simulations seems to indicate that the 500 K run gives the best description of experimental conditions at 300 K.

Figure 2 shows spectra computed from classical and CP−MD simulations at 300 K. The classical-short spectrum can be compared directly to the CP−MD spectrum because the structural sampling is the same. The general shape of the spectra are similar with the features evident in the CP−MD spectrum also present in those from the classical simulation. The $\pi_{\mathrm{nb}}\pi^*$ band is slightly lower in energy and is also broader. There is also some further broadening in the spectrum from the longer simulation. Analysis of the MD trajectories shows that there are some significant differences in the structural parameters between the CP−MD and classical simulations. In particular, the C−N bond length is significantly shorter in the classical MD simulation. However, the prediction of the gross features of the spectrum appear not very sensitive to the quality of the simulation. Table 3 shows the ensemble average predictions of the $n\pi^*$ and $\pi_{\mathrm{nb}}\pi^*$ excitation energies. These predicted excitation energies are sensitive to the simulation, with some significant differences arising between classical and CP−MD simulations. For all simulations, there is a decrease in the excitation energy compared to the values at the planar minimum energy
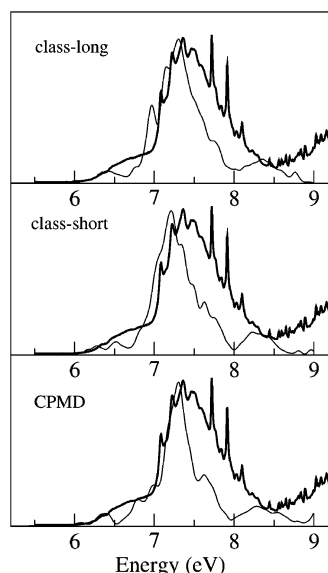
Figure 2. Theoretical simulations of the electronic absorption spectrum of formamide based on different MD simulations at 300 K. The experimental spectrum[13] is shown in bold.

Table 3. Ensemble Average $n\pi^*$ and $\pi_{nb}\pi^*$ Excitation Energies (in eV) and Oscillator Strengths in Parentheses

simulation	$n\pi^*$	$\pi_{nb}\pi^*$
CP-MD 300 K	5.61 (0.002)	7.27 (0.128)
CP-MD 400 K	5.63 (0.002)	7.28 (0.131)
CP-MD 500 K	5.57 (0.004)	7.28 (0.131)
classical (short) 300 K	5.74 (0.001)	7.23 (0.124)
classical (long) 300 K	5.72 (0.002)	7.23 (0.117)

Table 4. MRCI/d-aug-cc-pVDZ Excitation Energies, ΔE (in eV); Permanent and Transition Dipole Moments, μ and μ^T (in debye); and Oscillator Strengths, σ, for Formamidic Acid[a]

state	ΔE	μ_x	μ_y	μ_z	$|\mu|$	μ_x^T	μ_y^T	μ_z^T	σ	assignment
1A′		0.39	−1.38	0.00	1.43					G. S.
2A′	7.30	−2.62	0.80	0.00	2.73	0.05	1.17	0.00	0.038	n3s
3A′	7.74	−1.28	−0.15	0.00	1.29	−1.87	−0.88	0.00	0.125	$\pi_{nb}\pi^*$
4A′	8.02	0.41	−1.24	0.00	1.30	−0.96	−0.72	0.00	0.044	n3p
5A′	8.37	−0.48	4.22	0.00	4.25	0.15	1.14	0.00	0.042	n3p
6A′	8.80	5.35	−0.96	0.00	5.44	−2.07	−0.48	0.00	0.151	$\pi_{nb}3p$
7A′	9.10	0.45	−0.77	0.00	0.89	0.81	−0.45	0.00	0.032	n3d
8A′	9.20	0.38	−3.76	0.00	3.78	−0.05	0.09	0.00	0.000	n3d
9A′	9.26	6.66	−2.05	0.00	6.97	−0.28	−0.36	0.00	0.007	n3d
10A′	9.42	0.97	−1.50	0.00	1.78	0.22	−0.07	0.00	0.020	$\pi_{nb}3d$
1A″	6.77	1.61	0.05	0.00	1.61	0.00	0.00	0.70	0.012	$n\pi^*$
2A″	6.89	−0.56	−0.20	0.00	0.60	0.00	0.00	−0.49	0.006	$\pi_{nb}3s$
3A″	7.38	−0.69	0.20	0.00	0.72	0.00	0.00	0.69	0.013	$\pi_{nb}3p$
4A″	7.97	0.16	4.05	0.00	4.05	0.00	0.00	0.69	0.014	$\pi_{nb}3p$
5A″	8.41	−0.67	1.04	0.00	1.23	0.00	0.00	−0.58	0.011	n3p
6A″	8.63	−1.74	−1.16	0.00	2.09	0.00	0.00	0.36	0.004	$\pi_{nb}3d$
7A″	8.76	3.50	−4.01	0.00	5.32	0.00	0.00	0.58	0.011	$\pi_{nb}3d$
8A″	8.79	−0.60	−5.52	0.00	5.56	0.00	0.00	−0.09	0.000	$\pi_{nb}3d$

[a] The coordinates (in bohr) of the C, N, and O atoms are (0.17, −0.78, 0), (2.09, 0.68, 0), and (−2.21, 0.14, 0), respectively.
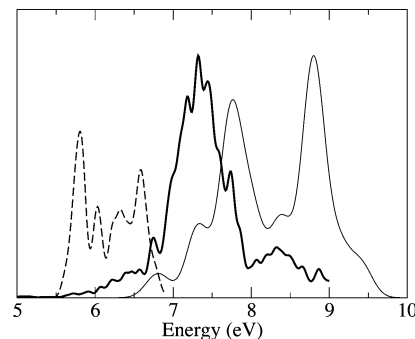

Figure 3. Theoretical simulations of the electronic absorption spectrum of formamide (bold line), formamidic acid (solid line), and ammonia (broken line).

structure. This has been attributed to the structure of the excited-state being nonplanar. Consequently, the nonplanar structures drawn from the simulation will tend to stabilize the excited state relative to the ground-state, resulting in a red shift.[15] However, this red shift is smaller than the typical values reported in earlier work.

Formamidic acid is formed by a proton transfer from the NH_2 group to the C=O group. In the gas phase, the barrier for this process is very large, but it is lowered significantly by hydrogen bonding.[39] Because formamidic acid is a possible contaminant, we have also computed its electronic spectrum to determine whether it accounts for remaining deficiencies in the computed spectrum. Table 4 shows the properties of the computed excited states. The calculations show that formamidic acid has a number of intense transitions, in particular, for the $\pi_{nb}\pi^*$ and $\pi_{nb}3p$ states. The $\pi_{nb}\pi^*$ transition is blue-shifted by 0.41 eV. A much larger change is observed for the 1A″ state, which is calculated to lie at 6.77 eV compared to 5.76 eV for formamide. This state is also labeled $n\pi^*$; however, the lone pair orbital is now associated with the nitrogen atom. Like formamide, there are also a number of additional Rydberg states with significant oscillator strengths. Figure 3 shows the electronic spectrum for formamidic acid. The spectrum indicates that formamidic acid would make little contribution to the spectrum on the low-energy side of the formamide $\pi_{nb}\pi^*$ band. However, formamidic acid does have intense transitions on the high-energy side of the formamide $\pi_{nb}\pi^*$ band.

It is interesting to note that the electronic spectrum of formamide in solution does show an intense band above 7.8 eV[5]. This band is not accounted for by condensed-phase ab initio calculations of formamide.[19,20] Formamidic acid is more likely to be present in solution and may provide a possible explanation for this band.

Ammonia is another contaminant that is likely to be present. Figure 3 shows a simulated 300 K spectrum for ammonia at low energies. This spectrum is based on MRCI/d-aug-cc-pVDZ on the 100 snapshots drawn from a CP−MD simulation. The spectrum shows that ammonia has an intense transition in the 5.5−7 eV region of the spectrum. This coincides with the low-energy shoulder of the $\pi_{nb}\pi^*$ band of formamide. In the experiment,[13] the effects of ammonia contamination were removed; however, it is likely that some residual effects remain. Another possible contaminant is dimers of formamide. Calculation of the excited states of a formamide dimer at the MRCI level (even with C_{2h} symmetry) with a suitable basis set and active space is currently beyond our computational resources.

Electronic Absorption Spectrum of Formamide

J. Chem. Theory Comput., Vol. 2, No. 6, 2006 **1603**

4. Conclusions

The simulation of the electronic absorption spectrum of formamide at finite temperatures has been investigated using a combination of CP−MD and high-level ab initio quantum chemistry. The excited states of formamide have been computed with MRCI. It is shown that, in conjunction with a sufficiently large basis set, the experimental excitation energies are reproduced accurately. To obtain a thermally broadened spectrum, we have averaged over a large number of single-point MRCI excitation spectra calculated for geometries sampled from a CP−MD simulation. Comparison of the computed spectra with the experimental spectrum at 300 K shows that spectra computed at 500 K yield a much better agreement with experimental results. One possible reason for this may be the absence of nuclear quantum effects in the simulation. Previous studies have shown that nuclear quantum fluctuations may be emulated by CP−MD simulations at higher temperatures.

The accuracy of the computed absorption spectrum has allowed other aspects of the experimental spectrum to be explored. The effects on the spectrum of possible contamination by ammonia and formamidic acid have been studied. Formamidic acid can contribute at high energies and may be important for electronic spectra of formamide measured in solution. Ammonia can also make significant contributions, in particular, to the shoulder region of the experimental formamide spectrum at 6.5 eV. Overall, the calculations demonstrate that electronic absorption spectra at finite temperatures can be simulated accurately from first principles using a combination of CP−MD and quantum chemistry. However, this remains a demanding task because accurate quantum chemistry in conjunction with extensive averaging over molecular structure is required.

References

(1) Chen, E. F.; Wittung-Stafshede, P.; Kliger, D. S. *J. Am. Chem. Soc.* **1999**, *121*, 3811.

(2) Rubstov, I. V.; Wang, J.; Hochstrasser, R. M. *J. Chem. Phys.* **2003**, *118*, 7733.

(3) Besley, N. A.; Hirst, J. D. *J. Am. Chem. Soc.* **1999**, *121*, 9636.

(4) Basch, H.; Robin, M. B.; Kuebler, N. A. *J. Chem. Phys.* **1967**, *47*, 1201.

(5) Basch, H.; Robin, M. B.; Kuebler, N. A. *J. Chem. Phys.* **1968**, *49*, 5007.

(6) Harding, L. B.; Goddard, W. A. *J. Am. Chem. Soc.* **1975**, *97*, 6300.

(7) Stenkamp, L. Z.; Davidson, E. R. *Theor. Chim. Acta* **1977**, *44*, 405.

(8) Nitzsche, L. E.; Davidson, E. R. *J. Chem. Phys.* **1978**, *68*, 3103.

(9) Oliveros, E.; Riviere, M.; Teichteil, C.; Malrieu, P. *Chem. Phys. Lett.* **1978**, *57*, 220.

(10) Hirst, J. D.; Hirst, D. M.; Brooks, C. L. *J. Phys. Chem.* **1996**, *100*, 13487.

(11) Serrano-Andrés, L.; Fülscher, M. *J. Am. Chem. Soc.* **1996**, *118*, 12190.

(12) Szalay, P. G.; Fogarasi, G. *Chem. Phys. Lett.* **1997**, *270*, 406.

(13) Gingell, J. M.; Mason, N. J.; Zhao, H.; Walker, I. C.; Siggel, M. R. F. *Chem. Phys.* **1997**, *220*, 191.

(14) Doltsinis, N. L.; Sprik, M. *Chem. Phys. Lett.* **2000**, *330*, 563.

(15) Besley, N. A.; Oakley, M. T.; Cowan, A. J.; Hirst, J. D. *J. Am. Chem. Soc.* **2004**, *126*, 13502.

(16) Del Bene, J. E. *J. Chem. Phys.* **1975**, *62*, 1961.

(17) Sobolewski, A. *Photochem. Photobiol.* **1995**, *89*, 89.

(18) Krauss, M.; Webb, S. P. *J. Chem. Phys.* **1997**, *107*, 5771.

(19) Besley, N. A.; Hirst, J. D. *J. Phys. Chem. A* **1998**, *102*, 10791.

(20) Besley, N. A.; Hirst, J. D. *J. Am. Chem. Soc.* **1999**, *121*, 8559.

(21) Rocha, R. R.; Martins, V. M.; Coutinho, K.; Canuto, S. *Theor. Chem. Acc.* **2002**, *108*, 31.

(22) Besley, N. A. *Chem. Phys. Lett.* **2004**, *390*, 124.

(23) Kumar P.; Marx, D. *Chem. Phys. Phys. Chem.* **2006**, *8*, 573.

(24) Marx, D.; Parrinello, M. *Z. Phys. D: At., Mol. Clusters* **1997**, *41*, 253.

(25) *CPMD 3.9*; MPI für Festkörperforschung: Stuttgart, Germany; IBM Zurich Research Laboratory: Zurich, Switzerland.

(26) Marx, D.; Hutter, J. In *Modern Methods and Algorithms of Quantum Chemistry*; Grotendorst, J., Ed.; NIC: Jülich, Germany, 2000. www.theochem.ruhr-uni-bochum.de/go/cprev.html (accessed Sept 2006).

(27) Becke, A. D. *Phys. Rev. A: At., Mol., Opt. Phys.* **1988**, *38*, 3098.

(28) Lee, C.; Yang, W.; Parr, R. C. *Phys. Rev. B: Condens. Matter Mater. Phys.* **1988**, *37*, 785.

(29) Troullier, N.; Martins, J. L. *Phys. Rev. B: Condens. Matter Mater. Phys.* **1991**, *43*, 1993.

(30) Nosé, S. *J. Chem. Phys.* **1984**, *81*, 511.

(31) Hoover, W. G. *Phys. Rev. A: At., Mol., Opt. Phys.* **1985**, *31*, 1695.

(32) Brooks, B. R.; Bruccoleri, R. E.; Olafson, B. D.; States, D. J.; Swaminathon, S.; Karplus, M. *J. Comput. Chem.* **1983**, *4*, 187.

(33) MacKerell, A. D.; Bashford, D.; Bellott, M.; Dunbrack, R. L.; Evanseck, J. D.; Field, M. J.; Fischer, S.; Gao, J.; Guo, H.; Ha, S.; Joseph-McCarthy, D.; Kuchnir, L.; Kuczera, K.; Lau, F. T. K.; Mattos, C.; Michnick, S.; Ngo, T.; Nguyen, D. T.; Prodhom, B.; Reiher, W. E.; Roux, B.; Schlenkrich, M.; Wiorkiewicz-Kuczera, J.; Yin, D.; Karplus, M. *J. Phys. Chem. B* **1998**, *102*, 3586.

(34) MOLPRO is a package of ab initio programs written by H.-J. Werner and P. J. Knowles, with contributions from J. Almlöf, R. D. Amos, A. Berning, M. J. O. Deegan, F. Eckert, S. T. Elbert, C. Hampel, R. Lindh, W. Meyer, A. Nicklass, K. Peterson, R. Pitzer, A. J. Stone, P. R. Taylor, M. E. Mura, P. Pulay, M. Schuetz, H. Stoll, T. Thorsteinsson, and D. L. Cooper.

(35) Knowles, P. J.; Werner, H.-J. *Theor. Chim. Acta* **1992**, *84*, 95.

(36) Dunning, T. H., Jr. *J. Chem. Phys.* **1989**, *90*, 1007.

(37) Kendall, R.; Dunning, T. H., Jr.; Harrison, R. J. *J. Chem. Phys.* **1992**, *96*, 6796.

(38) Woon, D. E.; Dunning, T. H., Jr. *J. Chem. Phys.* **1994**, *100*, 2975.

(39) Wang, X.-C.; Nichols, J.; Feyereisen, M.; Gutowski, M.; Boatz, J.; Haymet, A. D. J.; Simons, J. *J. Phys. Chem.* **1991**, *95*, 10419.